

MASS-LOSS RATE BY THE MIRA IN THE SYMBIOTIC BINARY V1016 CYGNI FROM RAMAN SCATTERING

M. SEKERÁŠ AND A. SKOPAL

Astronomical Institute, Slovak Academy of Sciences, 059 60 Tatranská Lomnica, Slovakia; sekeras@ta3.sk (MS), skopal@ta3.sk (AS)

Draft version June 22, 2015

ABSTRACT

The mass-loss rate from Mira variables represents a key parameter in our understanding of their evolutionary tracks. We introduce a method for determining the mass-loss rate from the Mira component in D-type symbiotic binaries via the Raman scattering on atomic hydrogen in the wind from the giant. Using our method, we investigated Raman He II $\lambda 1025 \rightarrow \lambda 6545$ conversion in the spectrum of the symbiotic Mira V1016 Cyg. We determined its efficiency, $\eta = 0.102, 0.148$, and the corresponding mass-loss rate, $\dot{M} = 2.0_{-0.2}^{+0.1} \times 10^{-6}, 2.7_{-0.1}^{+0.2} \times 10^{-6} M_{\odot} \text{ yr}^{-1}$, using our spectra from 2006 April and 2007 July, respectively. Our values of \dot{M} that we derived from Raman scattering are comparable with those obtained independently by other methods. Applying the method to other Mira–white dwarf binary systems can provide a necessary constraint in the calculation of asymptotic giant branch (AGB) evolution.

Keywords: binaries: symbiotic – scattering – stars: individual (V1016 Cyg) – stars: mass-loss

1. INTRODUCTION

Symbiotic stars are the widest interacting binaries that comprise a late-type cool component, which is a red/yellow giant or a Mira variable and a hot compact star, in most cases a white dwarf (WD). The WD accretes a fraction of the stellar wind from the giant, which makes it very hot ($\approx 10^5$ K) and luminous ($\approx 10^2 - 10^4 L_{\odot}$), and thus capable of ionizing the neutral wind from the giant, giving rise to the so-called symbiotic nebula (Seaquist et al. 1984, hereafter STB). Assuming a stationary binary during the quiescent phase, STB found that the neutral region usually has the shape of a cone, with the giant below its top, facing the WD. According to the spectral energy distribution in the IR region, we distinguish S-type (stellar) and D-type (dusty) symbiotic stars (Webster & Allen 1975). The former is represented by a stellar type of the IR continuum from a normal giant, whereas the latter contains an additional emission from the dust produced by an evolved Mira-type variable. D-type symbiotics are therefore called symbiotic Miras.

The environment of symbiotic stars is very suitable for observing the effects of Thomson, Rayleigh, and Raman-scattering processes (e.g. Schmid 1997). Thomson scattering by free electrons arises in the symbiotic nebula. Its effect on the broadening of strong emission lines was recently investigated by Sekeráš & Skopal (2012). The effects of Raman and Rayleigh scattering processes are observable when the radiation from/around the WD passes through the neutral part of the giant wind. In these processes a photon excites an atom from its ground state to an intermediate state, which is immediately stabilized by a transition to a true bound state. If this is followed by the immediate reemission of a photon of the same wavelength, we talk about Rayleigh scattering. If the stabilizing transition results in emitting a photon of a different frequency, we talk about Raman scattering. Raman scattering as a diagnostic tool in astrophysics was outlined by Nussbaumer et al. (1989).

The most famous example of Raman-scattered lines in the spectrum of symbiotic stars is represented by broad emission features at 6825 and 7082 Å that are formed when the photons of O VI 1032 and 1038 Å emission lines are scattered by neutral hydrogen atoms in the wind from the giant (Schmid 1989; Schmid et al. 1999). Also, transitions between the levels of even principal quantum numbers in the He II atom produce photons that can be easily scattered onto neutral hydrogen atoms because their wavelengths are near to the H I Lyman transitions, where the scattering cross-section is relatively large (e.g. Lee & Lee 1997; Lee 2012). In particular, the Raman emission at 6545 Å, produced by He II 1025 Å scattering, was observed in some planetary nebulae and symbiotic stars (e.g. Pequignot et al. 1997; Lee et al. 2001, 2003, 2006). Its cross-section is $8.05 \times 10^{-22} \text{ cm}^2$ (Lee 2009), which means that it operates in scattering regions with H I column density, $N_{\text{HI}} \gtrsim 10^{21} \text{ cm}^{-2}$. In symbiotic binaries the neutral material is supplied into the binary environment by the cool giant. Assuming the STB geometry of the neutral region, the Raman conversion process is related to its size, which depends on the mass-loss rate from the giant, \dot{M} (see STB). Therefore, Raman-scattered lines can provide an independent determination of \dot{M} .

In this paper we investigate the He II Raman-scattered emission at 6545 Å in our spectra of D-type symbiotic star V1016 Cyg. In 1964, V1016 Cyg underwent a nova-like outburst (McCuskey 1965). Its brightness is very slowly fading from its peak $V \sim 10.8$ mag in 1967–1970 to $V \sim 11.9$ mag in 2007 (e.g. Mürset & Nussbaumer 1994; Parimucha et al. 2002; Arkhipova et al. 2008). The binary is very extended, as given by its orbital period, estimated to be 6 – 544 years (e.g. Parimucha et al. 2002, and the references therein). Analysis of the ultraviolet spectrum revealed the presence of a very hot ($\approx 150,000$ K) and luminous ($\approx 30,000 L_{\odot}$) WD, whose radiation gives rise to a strong and extended symbiotic nebula by ionizing a fraction of the neutral wind from its

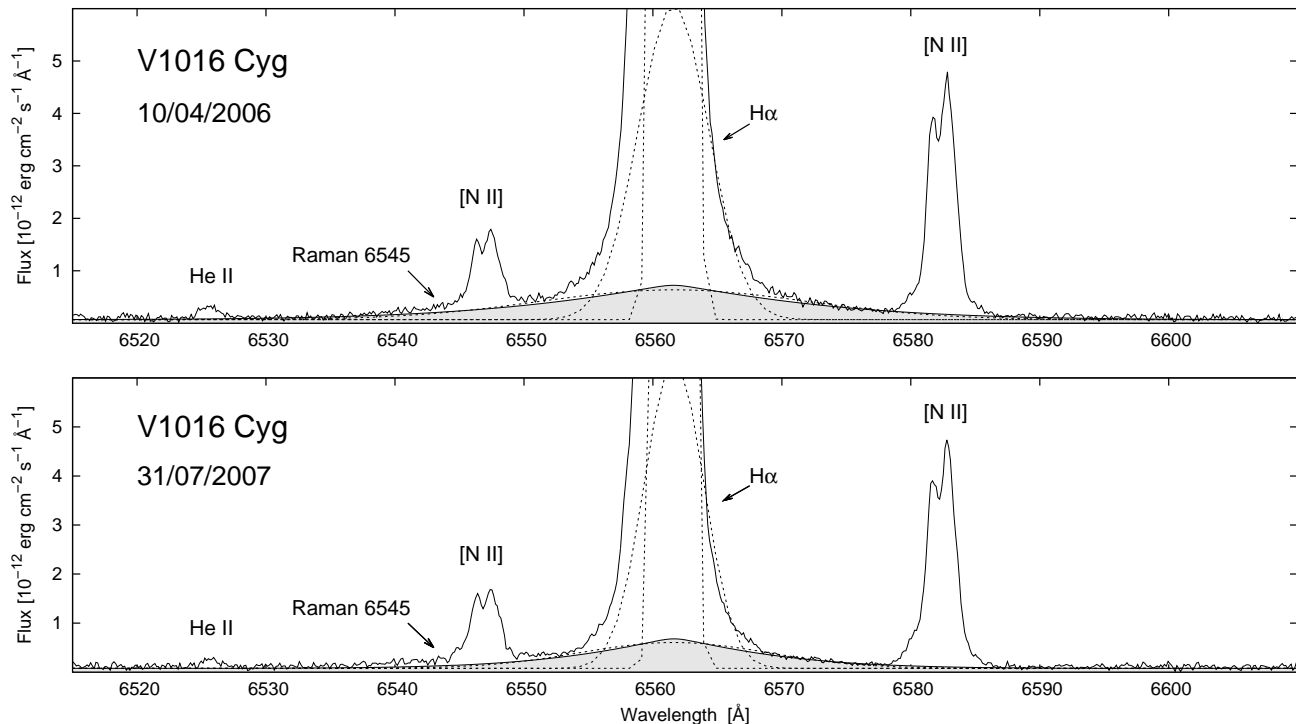


Figure 1. Our spectra of V1016 Cyg covering the vicinity of the $H\alpha$ line. Its profile was approximated by three Gaussians (dotted lines). The broadest Gaussian was matched by a scattering of $H\alpha$ photons on free electrons in the symbiotic nebula (shaded area). A slightly enhanced blue $H\alpha$ wing around the emission line [N II] 6548 Å indicates the possible presence of Raman 6545 Å emission.

Mira-type companion (e.g. Nussbaumer & Schild 1981; Schmid & Schild 1990; Mürset & Nussbaumer 1994).

In Section 3.1 we describe a method for isolating Raman-scattered emission at 6545 Å from the spectrum, and in Section 3.2.1 we determine the efficiency of the corresponding $\text{He II } \lambda 1025 \rightarrow \lambda 6545$ conversion. Assuming the basic ionization structure of V1016 Cyg (Section 3.3.1) we estimate \dot{M} from its cool component (Section 3.3.2). A discussion and our conclusions are found in Sections 4 and 5, respectively.

2. OBSERVATIONS

Four optical spectra (6420–6710 Å) of the symbiotic star V1016 Cyg were obtained at the David Dunlap Observatory of the University of Toronto by an 1.88-m telescope equipped with a single-dispersion slit spectrograph and the Jobin Yvon Horiba CCD detector (2048×512 pixels) at the Cassegrain focus. Two of them were obtained on 2006 April 10, with exposure times of 120 and 60 s, and two were obtained on 2007 July 31, with 100 and 60 s exposures. We combined the two spectra from each date to find both the continuum and the strong $H\alpha$ line in one spectrum. The resulting spectra were processed with basic procedures using the IRAF software package.

Near-simultaneous CCD photometry was obtained at the Stará Lesná observatory using the SBIG ST10 MXE CCD camera with the chip 2184×1472 pixels and the $UBV(RI)_C$ Johnson-Cousins filter set mounted at the Newtonian focus of a 0.5 m telescope (see Parimucha & Vaňko 2005, in detail). Magnitudes $U = 11.10$, $B = 11.96$, $V = 11.92$, $R_C = 10.55$, $I_C = 11.03$, and $U = 11.21$, $B = 12.09$, $V = 12.14$, $R_C = 10.73$, $I_C = 11.15$, were measured on 2006 April 8 and 2007 July

7, respectively.

Arbitrary units of the spectra were converted to fluxes in $\text{erg cm}^{-2} \text{s}^{-1} \text{Å}^{-1}$ using V and R_C magnitudes that were corrected for emission lines (see Skopal 2007). Their contribution to the true continuum was $\Delta R_C = -1.51$ and -1.26 mag in our spectra. The correction in the V filter was adopted from Table 2 of Skopal (2007). Magnitudes were converted to fluxes according to the calibration of Henden & Kaitchuck (1982). Finally, the spectra were corrected for interstellar reddening according to Cardelli et al. (1989) using the color excess $E_{B-V} = 0.28$ mag (Nussbaumer & Schild 1981).

3. ANALYSIS AND RESULTS

3.1. Disentangling of Emission Lines

Both spectra were dominated by a strong $H\alpha$ line with broad wings, with a total equivalent width of 4064 and 2764 Å, and FWHMs of 1.8 and 1.6 Å in 2006 April and 2007 July (see Figs. 1 and 2), respectively.

The slightly enhanced blue wing of $H\alpha$ around [N II] 6548 Å suggests the presence of Raman 6545 Å emission. To isolate it, we proceeded similarly as Lee et al. (2003). First, we approximated the continuum by a linear function. Then we removed contributions from the $H\alpha$ wing, and the $\text{He II } 6560$ Å and [N II] 6548 Å lines. All profiles were approximated by Gaussian functions (Figs. 1–3).

- i. The $H\alpha$ line was fitted by three Gaussians with the same central wavelength. The first curve fits the strong and relatively narrow core of the line ($FWHM \sim 1.7$ Å), whose origin can be connected with the ionized wind from the giant. The second curve extracts a fainter but broader compo-

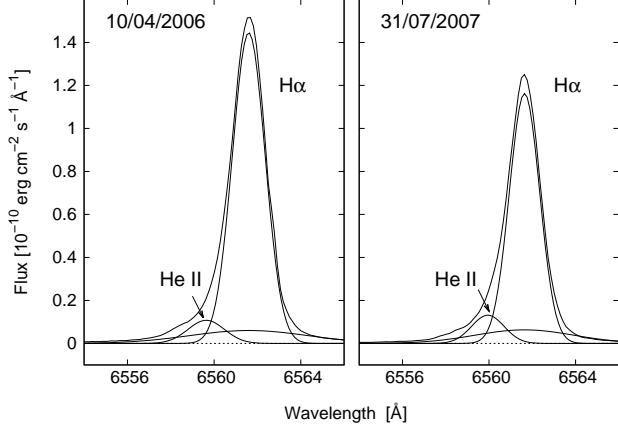


Figure 2. Observed profile of the H α line (thick line). Its components are denoted by thin lines, including the He II 6560 Å line.

ment ($FWHM \sim 6 \text{ \AA}$), probably formed in the wind from the burning WD (see Skopal 2006). The third Gaussian matches the faint and very extended wings ($FWHM \sim 21 \text{ \AA}$), which can be caused by a scattering of free electrons (see Sekeráš & Skopal 2012), but a contribution from the Raman scattering of the continuum around Ly β cannot be excluded (e.g. Lee 2000).

- ii. The [N II] 6583 and 6548 Å lines consist of three components; a double-peaked core with a broad base. Therefore, we fitted their profiles with three Gaussians and subtracted the [N II] 6548 Å line using the ratio $F_{6583}/F_{6548} \sim 3$ (e.g. Storey & Zeppen 2000).
- iii. The He II 6560 Å line was fitted by a single Gaussian to tune the composite H α line profile at its blue side (Figure 2).

Finally, subtracting the above mentioned contributions from the spectrum, we isolated the Raman 6545 Å emission (see Figs. 3 and 4). Parameters of all fitted emission lines are in Table 1.

3.2. Raman-scattered He II 6545 Å Emission

According to the energy conservation of the Raman transition $\lambda_{1025} \rightarrow \lambda_{6545}$,

$$\lambda_R^{-1} = \lambda_i^{-1} - \lambda_{Ly\alpha}^{-1}, \quad (1)$$

where λ_R is the wavelength of the Raman-scattered emission at 6545 Å, λ_i is the wavelength of the incident photons of the He II 1025 Å line, and $\lambda_{Ly\alpha}$ is the wavelength of the Ly α line. Differentiating Equation (1), we get,

$$\frac{\Delta \lambda_R}{\lambda_R} = \frac{\lambda_R}{\lambda_i} \frac{\Delta \lambda_i}{\lambda_i}. \quad (2)$$

Hence the Raman-scattered feature is broadened with respect to the incident emission line by a factor of $(\lambda_R/\lambda_i)^2 \approx 40.8$ in the wavelengths space or $\lambda_R/\lambda_i \approx 6.4$ in the radial velocity space.

Lee et al. (2006) calculated the central wavelengths of the He II 6560 Å and Raman 6545 Å emission lines as $\lambda_{HeII} = 6560.13 \text{ \AA}$ and $\lambda_{Ram} = 6544.53 \text{ \AA}$, setting the position of the Raman 6545 Å emission to 15.6 Å blue-

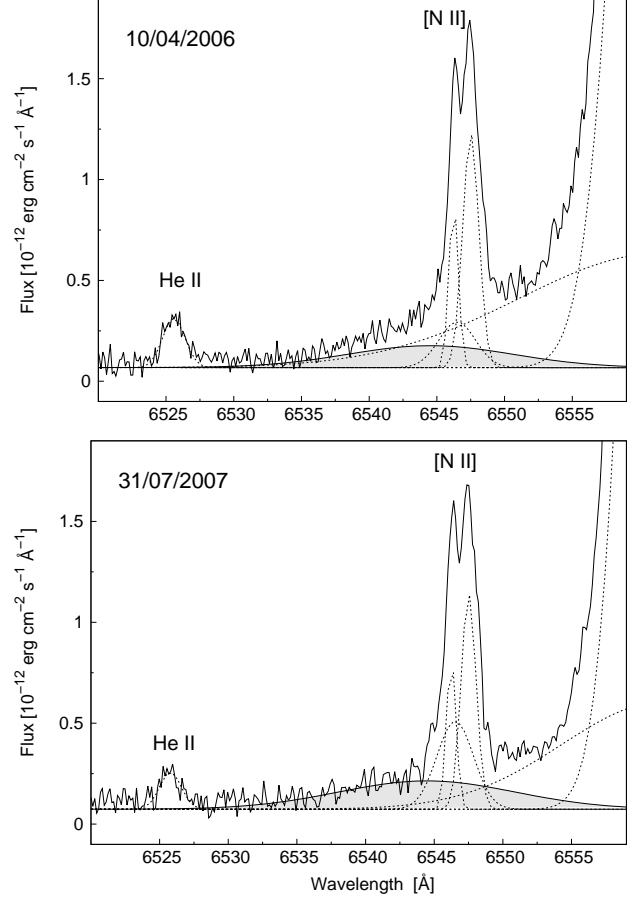


Figure 3. Raman 6545 Å emission (shaded area) blended in the wings of H α and [N II] 6548 Å lines. Their profiles were approximated by Gaussian functions (dotted lines, Section 3.1).

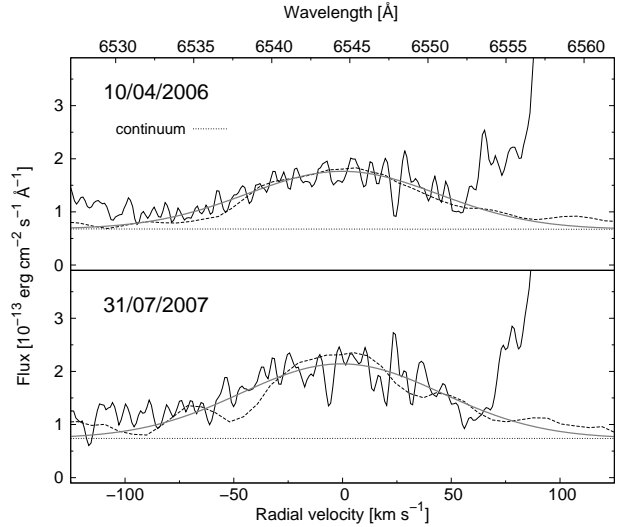


Figure 4. Isolated Raman-scattered 6545 Å emission feature (thick line) matched by the Gaussian function (gray line). It is compared with the He II 6527 Å line profile (dashed line). The radial velocity scale corresponds to the velocity space of the ordinary lines. The flux of the lines is normalized to the same total flux (see Section 4.3).

Table 1
Gaussian fit parameters of the Used Emission Lines (see Section 3.1).

Emission Line	2006 Apr			2007 Jul		
	λ_0 (Å)	F_0 ($\text{erg cm}^{-2} \text{s}^{-1} \text{Å}^{-1}$)	FWHM (Å)	λ_0 (Å)	F_0 ($\text{erg cm}^{-2} \text{s}^{-1} \text{Å}^{-1}$)	FWHM (Å)
He II	6525.6	2.4×10^{-13}	1.9	6525.7	1.8×10^{-13}	1.9
Raman He II 6545	6544.5	1.1×10^{-13}	14.5	6544.5	1.4×10^{-13}	15.2
[N II]	6546.2	8.2×10^{-13}	0.8	6546.2	7.5×10^{-13}	0.8
	6546.5	2.3×10^{-13}	3.2	6546.5	4.4×10^{-13}	3.1
	6547.5	1.2×10^{-12}	1.4	6547.5	1.1×10^{-12}	1.3
He II	6559.6	1.1×10^{-11}	2.0	6559.9	1.1×10^{-11}	1.8
H α	6561.6	1.4×10^{-10}	1.8	6561.6	1.2×10^{-10}	1.6
	6561.6	5.7×10^{-13}	24.7	6561.6	5.3×10^{-13}	17.3
	6561.6	6.0×10^{-12}	6.4	6561.6	6.3×10^{-12}	5.4
[N II]	6581.6	2.4×10^{-12}	0.8	6581.6	2.2×10^{-12}	0.8
	6582.3	1.0×10^{-12}	3.7	6582.1	1.5×10^{-12}	3.6
	6582.9	3.5×10^{-12}	1.4	6582.9	3.2×10^{-12}	1.3

Note. Denotation of parameters is given by the Gaussian function, $F_0 \exp(-0.5(\lambda - \lambda_0)^2/\sigma^2)$ and $\text{FWHM} = 2\sigma\sqrt{2\ln 2}$.

ward of the He II 6560 Å line. However, the exact position depends on several factors, e.g. a relative motion of the scattering and emitting regions and/or the column density of the neutral hydrogen (Jung & Lee 2004). The emission feature, which we extracted from the blue wing of the H α line, is shifted by 15.1 and 15.4 Å with respect to the He II 6560 Å line in our spectra from 2006 and 2007, respectively. Therefore, its position and the width (Table 1, Figure 4) imply that it is indeed the Raman-scattered He II 1025 Å line at 6545 Å.

3.2.1. Efficiency of Raman He II $\lambda 1025 \rightarrow \lambda 6545$ Scattering

The Raman-scattering efficiency, η , is defined as the photon ratio between the Raman-scattered, N_{6545} , and the original He II 1025 Å line photons, N_{1025} ,

$$\eta = \frac{N_{6545}}{N_{1025}}. \quad (3)$$

According to Lee et al. (2003), this can be expressed as

$$\eta = \frac{F_{6545}/h\nu_{6545}}{F_{1025}/h\nu_{1025}} = \frac{F_{6545}/h\nu_{6545}}{F_{6560}/h\nu_{6560}} \frac{F_{6560}/h\nu_{6560}}{F_{1025}/h\nu_{1025}}, \quad (4)$$

where F_{6560} is the flux of the He II 6560 Å emission line. This approach takes advantage of the fact that even though we have no observation of the original He II 1025 Å line, we can still determine the efficiency using the observed He II 6560 Å line located close to Raman 6545 Å emission (Figure 2). According to Gurzadyan (1997), under case B of recombination for the electron temperature $T_e = 20,000 \text{ K}$, theoretical fluxes of the referred He II lines in Equation (4) are $F_{6560} = 0.135 F_{4686}$ and $F_{1025} = 0.618 F_{4686}$, where F_{4686} is the total flux of the He II 4686 Å line. Assuming an isotropic He II-emitting region, the Raman-scattering efficiency $\eta = 0.102$ and 0.148 in 2006 April and 2007 July, respectively. For $T_e = 10,000 \text{ K}$, η will increase to 0.129 and 0.187 , respectively.

3.2.2. Covering factor of the scattering region

Lee (2009) determined the cross-section of the Raman He II $\lambda 1025 \rightarrow \lambda 6545$ conversion to $\sigma_{\text{Ram}} = 8.05 \times 10^{-22} \text{ cm}^2$. The corresponding optical depth is

$$\tau_{\text{Ram}} = N_{\text{HI}} \sigma_{\text{Ram}}, \quad (5)$$

where N_{HI} is the column density of the neutral hydrogen region along the line of the incident He II 1025 Å photons. This implies that for $N_{\text{HI}} > 1.24 \times 10^{21} \text{ cm}^{-2}$ (i.e. $\tau_{\text{Ram}} > 1$), the H I region becomes optically thick for Raman scattering. Performing a detailed Monte Carlo calculations, Lee (2000) found that in the optically thick region the scattering efficiency reaches a maximum value of 0.6. This means that 60% of all photons entering the optically thick scattering region, N_{1025}^e , are converted to Raman 6545 Å photons, i.e.,

$$0.6 N_{1025}^e = N_{6545}. \quad (6)$$

A part of the H I region, which is optically thick for the He II 1025 Å Raman-scattering, defines a covering factor C_S as (Equations (3) and (6)),

$$C_S = \frac{N_{1025}^e}{N_{1025}} = \frac{\eta}{0.6}, \quad (7)$$

which represents a fraction of the sky, seen from the He II emission zone, covered by the Raman scattering region. For the whole sphere, $C_S = 1$. From our spectra, we determined the covering factors to be 0.171 and 0.248.

3.3. Mass-loss Rate from the Giant

3.3.1. Ionization Model

In the STB model, the boundary between the neutral and ionized part of the wind from the giant is represented by a locus of points, where the flux of hydrogen-ionizing photons from the hot star, L_{H} , is balanced by the rate of recombinations in the giant's wind. In the WD-centered polar coordinate system (s, θ), this equilibrium condition can be expressed as (Nussbaumer & Vogel 1987),

$$L_{\text{H}} = 4\pi \int_0^{s\theta} (1 + a(\text{He})) n_{\text{H}}^2(s) \alpha_{\text{B}}(\text{H}, T_e) s^2 ds, \quad (8)$$

where s_θ is the distance to the H I/H II boundary from the WD for a given θ , $a(\text{He})$ is the abundance by number of helium atoms, $n_{\text{H}}(s)$ is the concentration of hydrogen atoms, and $\alpha_{\text{B}}(\text{H}, T_e)$ is the total recombination coefficient for hydrogen atoms in case B ($\text{cm}^3 \text{s}^{-1}$). The STB model assumes a stationary symbiotic binary with a spherically symmetric wind flowing from the giant at a constant velocity, v_∞ . Such a wind obeys the continuity equation

$$\dot{M} = 4\pi\mu m_{\text{H}} n_{\text{H}}(r) v_\infty, \quad (9)$$

where \dot{M} is the mass-loss rate from the giant, r is the distance from its center, μ is the mean molecular weight, and m_{H} is the mass of the hydrogen atom. In the reference system of the WD,

$$r = \sqrt{s^2 + p^2 - 2sp \cos \theta}, \quad (10)$$

where p is the binary separation. Following these equations, the H I/H II interface is given by the solution of a parametric equation (see Nussbaumer & Vogel 1987),

$$f(u, \theta) = X_{\text{H}^+}, \quad (11)$$

where $u = s/p$, the parameter

$$X_{\text{H}^+} = \frac{4\pi\mu^2 m_{\text{H}}^2}{\alpha_{\text{B}}(\text{H}, T_e)(1 + a(\text{He}))} p L_{\text{H}} \left(\frac{v_\infty}{\dot{M}} \right)^2, \quad (12)$$

and the function

$$f(u, \theta) = \int_0^{u_\theta} \frac{u^2}{(u^2 - 2u \cos \theta + 1)^2} \left(\frac{v_\infty}{v(r)} \right)^2 du, \quad (13)$$

where, instead of the constant velocity, we used the β -law wind velocity profile (Lamers & Cassinelli 1999)

$$v(r) = v_0 + (v_\infty - v_0) \left(1 - \frac{R_g}{r} \right)^\beta. \quad (14)$$

The initial velocity $v_0 = v(R_g)$, where R_g is the radius of the giant, v_∞ is the wind terminal velocity, and the parameter β determines the steepness of the velocity law. The value of v_0 is often linked to the isothermal speed of sound (Puls et al. 2008).

The setting of the STB model results in a symmetric ionization boundary with respect to the binary axis, whose shape is determined solely by the parameter X_{H^+} .

3.3.2. Mass-loss Rate from Raman Scattering

According to the meaning of the covering factor (see Section 3.2.2), we can express it via a solid angle Ω , under which the initial He II line photons, located mostly in the vicinity of the WD, can see the scattering region, i.e.

$$C_{\text{S}} = \frac{\Omega}{4\pi} = \frac{1 - \cos \theta_{\text{R}}}{2}. \quad (15)$$

Our values of C_{S} , 0.171 and 0.248, correspond to the opening angle of the Raman-scattering region $\theta_{\text{R}} = 48.9^\circ$ and 59.7° for the spectra from 2006 April and 2007 July. For a given STB model, the parameter X_{H^+} is related to the angle between the binary axis and the asymptote to the ionization boundary, θ_a (see Figure 6), as

$$X_{\text{H}^+} = \lim_{u \rightarrow \infty} f(u, \theta) = f(\theta_a). \quad (16)$$

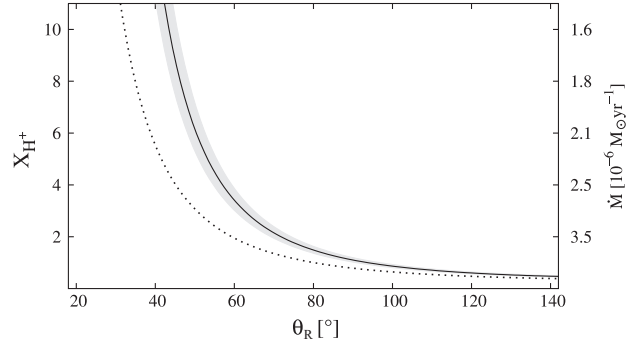


Figure 5. Parameter X_{H^+} as a function of the angle θ_{R} , which limits the Raman-scattering H I region (Equation (18)). The dotted line represents the model for a constant wind velocity ($v_\infty = 11 \text{ km s}^{-1}$), while the solid line represents the β -law wind (Equation (14)). The shaded area mirrors the uncertainty in R_g ($\pm 73 R_\odot$). The angle θ_{R} determines X_{H^+} and \dot{M} (Equation (20)), the scale of which is given on the y2-axis.

The covering factor of the total H I zone is larger than C_{S} , i.e. $\theta_a > \theta_{\text{R}}$, because the scattering region represents only a part of the whole H I region, which is optically thick for Raman scattering. In other words, the Raman-scattering H I region is located inside the whole H I zone because its angular extension θ_{R} is bounded by the column densities

$$N_{\text{HI}}(\theta) > 1.24 \times 10^{21} \text{ cm}^{-2} \quad (17)$$

(see Section 3.2.2). Therefore, to find the ionization boundary of the total H I zone (i.e. the X_{H^+} parameter in the STB model) from the size of the Raman-scattering H I zone, we have to determine X_{H^+} as a function of θ_{R} taking into account the condition (17). For this purpose we reconstruct the relation,

$$X_{\text{H}^+} = \lim_{u \rightarrow u_{\text{R}}} f(u, \theta) = f(\theta_{\text{R}}), \quad (18)$$

where u_{R} is the distance between the WD and the H I/H II interface in the line θ_{R} , which satisfies the condition,

$$N_{\text{HI}}(\theta_{\text{R}}) = \int_{u_{\text{R}}}^{\infty} n_{\text{H}}(u, \theta_{\text{R}}) du = 1.24 \times 10^{21} \text{ cm}^{-2}. \quad (19)$$

The concentrations $n_{\text{H}}(u, \theta)$ are calculated according to Equations (9)–(14) along the line θ throughout the H I region to infinity (in practice to $u = 1000$). In the calculation, \dot{M} in Equation (9) is parameterized by X_{H^+} (Equation (12)) as

$$\dot{M} = \left(\frac{\zeta}{X_{\text{H}^+}} \right)^{1/2}. \quad (20)$$

For V1016 Cyg, $p = 1.15 \times 10^{14} \text{ cm}$, as given by the orbital period of 15.1 years (Parimucha et al. 2002) and the total mass of the binary, $\equiv 2 M_\odot$, $L_{\text{H}} = 1.73 \times 10^{48} \text{ s}^{-1}$, $\alpha_{\text{B}}(\text{H}, T_e) = 1.43 \times 10^{-13} \text{ cm}^3 \text{ s}^{-1}$ (for $T_e = 20,000 \text{ K}$), $a(\text{He}) \equiv 0.15$ (Nussbaumer & Vogel 1987; Mürset & Nussbaumer 1994), and $v_\infty = 11 \text{ km s}^{-1}$ (Lee & Kang 2007), yield $\zeta = 1.05 \times 10^{41}$ (in units of cm g s). In the β -law wind (Equation (14)) we used the average radius of the Mira-variable, $R_g = 407 \pm 73 R_\odot$, as the results from the P-L relation of Mira variables in the LMC (Whitelock et al. 2009, 2013), the period

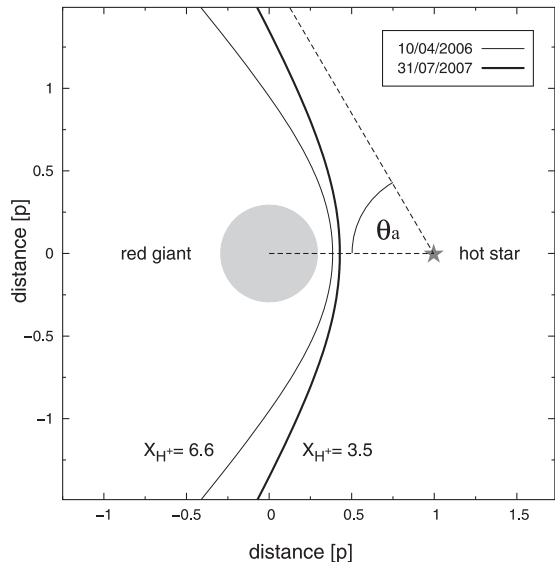


Figure 6. Ionization boundaries determined from the Raman-scattered 6545 Å emission feature observed in our spectra of V1016 Cyg. The neutral region is on the side of the boundary containing the giant. The asymptotic angle θ_a (Equation (16)) to the boundary $X_{H^+} = 3.5$ is shown for comparison.

of 474 days (Parimucha et al. 2002), and its average effective temperature of 2700 ± 200 K (from our model SED; in preparation). Furthermore, we adopted $\beta = 2.5$ (Schröder 1985) and $v_0 = 4.0 \pm 0.2 \text{ km s}^{-1}$ (\approx the sound speed in the giant’s atmosphere), where uncertainties in R_g and v_0 reflect those found in the temperature of the cool component.

Figure 5 shows the function $X_{H^+}(\theta_R)$ calculated according to Equation (18). Our values of $\theta_R = 48.9^\circ$ and 59.7° , as determined from the spectra in 2006 April and 2007 July, correspond to $X_{H^+} = 6.6$ and 3.5 for the β -law wind and 3.3 and 2.0 for the constant wind, respectively. Corresponding ionization boundaries for the β -law wind are shown in Figure 6. Finally, according to Equation (20) we obtained $\dot{M} = 2.0$ and $2.7 \times 10^{-6} M_\odot \text{ yr}^{-1}$ for the β -law wind, and $\dot{M} = 2.8$ and $3.6 \times 10^{-6} M_\odot \text{ yr}^{-1}$ for a constant velocity wind with $v_\infty = 11 \text{ km s}^{-1}$. The results are summarized in Table 2.

4. DISCUSSION

4.1. On the Difference Between the Angle θ_a and θ_R

The angle $\Delta\theta = \theta_a - \theta_R > 0$ cut out a fraction of the HI zone, where the Raman He II $\lambda 1025 \rightarrow \lambda 6545$ conversion can be neglected (i.e. $\tau_{\text{Ram}} < 1$). In our models, $\Delta\theta \lesssim 0.2^\circ$, which means that both the Raman-scattering HI region and the total HI region are nearly identical. As a result, the function $X_{H^+}(\theta_a)$ would also be nearly identical with the function $X_{H^+}(\theta_R)$ plotted in Figure 5. In such a case, we can set $\theta_R = \theta_a$, and obtain \dot{M} more easily by determining the parameter X_{H^+} directly with the aid of Equation (16).

The case $\theta_a \gg \theta_R$ can happen for low values of \dot{M} and L_H that result in low values of column densities $N_{\text{HI}}(\theta)$. Figure 7 shows such an example (model “ $N_{\text{HI}}(X=10)$ ”) together with the column densities of our

Table 2
Mass-loss Rates from the Mira-variable in V1016 Cyg as determined from He II 1025 Å Raman Scattering

Date	η (%)	C_S	θ_R ($^\circ$)	X_{H^+}	$\dot{M}/10^{-6}$ ($M_\odot \text{ yr}^{-1}$)
2007 Jul 31	14.8	0.24	59.7	3.5	$2.7^{+0.2}_{-0.1}$ ^a
				2.0	3.6^b
2006 Apr 10	10.2	0.17	48.9	6.6	$2.0^{+0.1}_{-0.2}$ ^a
				3.3	2.8^b
2002 May 20	17.0	0.28	64.0	2.8	$3.0^{+0.2}_{-0.2}$ ^c

Notes. Parameters η , C_S , θ_R , X_{H^+} and \dot{M} are given by Equations (4), (7), (15), (18) and (20), respectively.

^a β -law wind.

^b Constant velocity wind of 11 km s^{-1} .

^c For $\eta = 17\%$ of Lee et al. (2003).

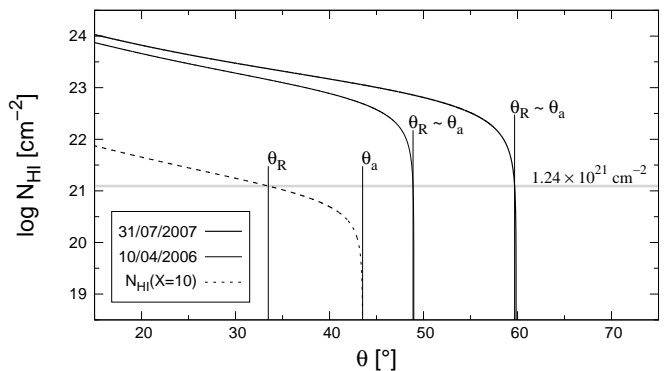


Figure 7. Column densities $N_{\text{HI}}(\theta)$ throughout the total HI region above the giant photosphere (i.e. $\theta > 13.8^\circ$). The asymptotic angle θ_a corresponds to the tangent of the function $N_{\text{HI}}(\theta)$, while the angle θ_R denotes the intersection of $N_{\text{HI}}(\theta)$ with the critical column density for He II 1025 Å Raman scattering (horizontal gray line, Equation (19)).

solutions. $N_{\text{HI}}(\theta)$ functions were calculated according to Equation (19), omitting the condition for the Raman-scattering limit, and for $\theta > 13.8^\circ$, i.e., above the giant’s photosphere. In all cases, the function $N_{\text{HI}}(\theta)$ has a maximum just above the giant, then gradually decreases, and steeply drops to zero for $\theta \rightarrow \theta_a$. The example model “ $N_{\text{HI}}(X=10)$ ” corresponds to $X_{H^+} = 10.0$ (i.e. $\theta_a = 43.5^\circ$), $\dot{M} = 2.0 \times 10^{-8} M_\odot \text{ yr}^{-1}$, $L_H = 2.7 \times 10^{44} \text{ s}^{-1}$, and other parameters as above. Its $N_{\text{HI}}(\theta)$ function crosses the limiting value at $\theta_R = 33.5^\circ$, i.e., $\Delta\theta = 10.0^\circ$. Figure 8 demonstrates a more general case, where the angle $\Delta\theta$ is a function of \dot{M} and L_H , which give the same value of $X_{H^+} = 6.6$. The figure shows that massive winds flowing at rates of $\sim 10^{-6} M_\odot \text{ yr}^{-1}$ have very small $\Delta\theta$ for He II 1025 Å scattering.

4.2. Comparison with Previous \dot{M}

Similar values of the mass-loss rate from the giant in V1016 Cyg were derived by different methods. Based on the far-IR colors, as measured during the IRAS survey, Kenyon et al. (1988) derived $\dot{M} = 6.3 \times 10^{-6} M_\odot \text{ yr}^{-1}$ for the distance of 2.1 kpc. Measuring the flux density at 3.6 cm, Seaquist et al. (1993) determined $\dot{M} = 1.3 \times$

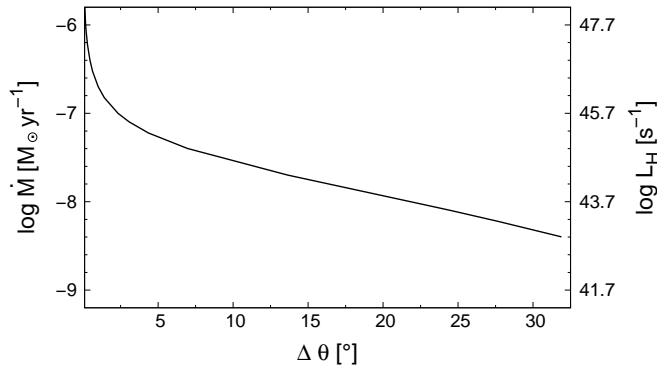


Figure 8. \dot{M} and L_H that correspond to $X_{H^+} = 6.6$ (Equation (12)) as a function of $\Delta\theta$ (see Section 4.1).

$10^{-5} M_{\odot} \text{ yr}^{-1}$ for the distance of 3.9 kpc. In both cases a constant wind velocity of 30 km s^{-1} was assumed. The latter value was obtained within the context of the STB model, where $\dot{M} \propto v_{\infty}$. This allows us to convert \dot{M} to $4.8 \times 10^{-6} M_{\odot} \text{ yr}^{-1}$ for $v_{\infty} = 11 \text{ km s}^{-1}$. We note that \dot{M} values derived from the radio emission can be overestimated because of the presence of the ionized wind from the hot component (e.g. Skopal 2006). By modeling the infrared excess emission of Mira variables in globular clusters, Frogel & Elias (1988) derived typical values of \dot{M} to be of $5 \times 10^{-6} M_{\odot} \text{ yr}^{-1}$.

In our approach we used the binary separation $p = 7.7 \text{ AU}$ (Section 3.3.2). Analyzing *Hubble Space Telescope* images of V1016 Cyg, Brocksopp et al. (2002) estimated a projected binary separation of $84 \pm 2 \text{ AU}$ (a distance of 2 kpc was assumed), which corresponds to an extremely long orbital period of ~ 544 years. For a comparison, recalculating \dot{M} for $p = 84 \text{ AU}$ by our method (keeping the covering factor unchanged) yields $\dot{M} = 9.1 \times 10^{-6}$ and $1.2 \times 10^{-5} M_{\odot} \text{ yr}^{-1}$ for the spectrum from 2006 and 2007, respectively. Thus, a significant enlargement of p by a factor of ~ 11 increases \dot{M} with a factor of ~ 4.5 only.

Finally, Lee et al. (2003) determined the efficiency of the $\text{He II } \lambda 1025 \rightarrow \lambda 6545$ conversion to $\eta = 0.17$ (i.e., $C_S = 0.28$ and $\theta_R = 64^\circ$) from the spectrum obtained on 2002 May 20. Applying our method to this value, we obtained $X_{H^+} = 2.8$ and $\dot{M} = 3.0 \times 10^{-6} M_{\odot} \text{ yr}^{-1}$, which is comparable to our results (see Table 2).

4.3. A Velocity Dispersion of the Giant's Wind

Figure 4 shows a comparison of the Raman-scattered $\text{He II } \lambda 6545 \text{ \AA}$ line with the ordinary $\text{He II } \lambda 6527 \text{ \AA}$ line. The weakness of the $\lambda 6545$ emission does not allow us to distinguish any more complex structures of its profile. Therefore, we matched it by a single Gaussian curve. Although there is no appropriate original $\text{He II } \lambda 1025 \text{ \AA}$ line,¹ we can still compare the $\lambda 6545$ line profile with other He II lines because they are formed in the same He^{++} region around the WD and thus are similar in the profile.

We determined the FWHM of the Raman feature to 14.5 and 15.2 \AA (Table 1), which, according to Equation (2), converts to the velocity widths $\Delta v \sim 104$ and $\sim 109 \text{ km s}^{-1}$. For $\text{He II } \lambda 6560 \text{ \AA}$, $\Delta v \sim 91$ and $\sim 82 \text{ km s}^{-1}$

in 2006 and 2007. The velocity width of the $\text{He II } \lambda 6527 \text{ \AA}$ line is $\sim 87 \text{ km s}^{-1}$ in both spectra. Hence, Δv of the Raman emission is larger by $\approx 20 \text{ km s}^{-1}$. Assuming a single-peaked profile of the original $\text{He II } \lambda 1025 \text{ \AA}$ line, this additional broadening can be attributed to the Doppler effect produced by the motion of the scattering H^0 -atoms relative to the He^{++} region. Basically, the neutral part of the wind between the two stars moves toward the He^{++} region and thus produces blue shifted Raman photons, while the outer wind region moves away from it, producing Raman photons in the red line wing (Schmid et al. 1999). This result suggests a dispersion velocity of the giant's wind to be of $\approx 20 \text{ km s}^{-1}$, which can be interpreted as double that of v_{∞} because it is consistent with a typical terminal velocity of the wind from Mira variables (e.g. Schild 1989; Vassiliadis & Wood 1993).

However, future repeated observations that are also made for other symbiotic Miras and for other Raman-scattered He II lines should allow us to obtain more accurate results.

5. CONCLUSIONS

In symbiotic binaries the He II emission is located predominantly near the hot component. A part of its line photons can be converted by atomic hydrogen in the neutral part of the giant's wind into Raman photons. Within the STB model (Section 3.3.1) the neutral region has a conical shape, whose opening angle is given by the flux of hydrogen-ionizing photons and the mass-loss rate from the giant. Therefore, by knowing the fundamental parameters of the hot component, the mass-loss rate can be probed via Raman scattering. The key parameter is the efficiency η of this process, because it is a function of the opening angle of the neutral zone. The method is described in Section 3.3.

In this paper we investigated Raman $\text{He II } \lambda 1025 \rightarrow \lambda 6545$ conversion in the spectrum of D-type symbiotic star V1016 Cyg. To isolate the Raman 6545 \AA emission and to derive η of the corresponding $\text{He II } \lambda 1025 \text{ \AA}$ scattering, we proceeded in a way that was similar Lee et al. (2003). In our spectra from 2006 April and 2007 July, we derived $\eta = 0.102$ and 0.148 . Using our method, we determined the corresponding $\dot{M} = 2.0^{+0.1}_{-0.2} \times 10^{-6}$ and $2.7^{+0.2}_{-0.1} \times 10^{-6} M_{\odot} \text{ yr}^{-1}$. The parameters are summarized in Table 2. Our quantities of \dot{M} are well comparable with those obtained by other methods (see Section 4.2).

Deriving \dot{M} by using $\text{He II } \lambda 1025 \text{ \AA}$ scattering has two main advantages: (i) a large σ_{Ram} (i.e., a low Raman-limiting H I column density) allows us to simplify the method by setting $\theta_R = \theta_a$ for sufficiently massive winds (Section 4.1, Figure 7); and (ii) the efficiency of $\text{He II } \lambda 1025 \text{ \AA}$ scattering can be derived just from the optical spectrum (Section 3.2.1).

The relative simplicity and accuracy of our method can be used to test, for example, a possible dependence of \dot{M} on the pulsation phase in symbiotic Miras. An extension of the method to other Mira-WD binary systems may probe theoretical predictions of \dot{M} at different stages of AGB evolution.

We thank the anonymous referee for useful comments and Theodor Pribulla for the acquisition of the optical

¹ The $\text{He II } \lambda 1025 \text{ \AA}$ line is severely blended with the geocoronal $\text{Ly}\beta$ emission on the only *FUSE* spectrum, No. A1340302000

spectra that we used in this contribution. This article was created through the realization of the project ITMS No. 26220120009, based on the supporting operational Research and development program financed by the European Regional Development Fund, which is also supported by the Slovak Academy of Sciences under a grant VEGA No. 2/0002/13.

Facility: David Dunlap Observatory.

REFERENCES

- Arhipova, V. P., Esipov, V. F., Ikonnikova, N. P., & Komissarova, G. V., 2008, *AstL*, 34, 474
- Brocksopp, C., Bode, M. F., Eyres, S. P. S., et al., 2002, *ApJ*, 571, 947
- Cardelli, J. A., Clayton, G. C., & Mathis, J. S., 1989, *ApJ*, 345, 245
- Frogel, J. A., & Elias, J. H., 1988, *ApJ*, 324, 823
- Gurzadyan, G. A., 1997, *The Physics and Dynamics of Planetary Nebulae*. (Berlin: Springer)
- Henden, A. A., & Kaitchuck, R. H., 1982, *Astronomical Photometry*. (New York: Van Nostrand Reinhold Company)
- Jung, Y-Ch., & Lee, H-W., 2004, *MNRAS*, 350, 580
- Kenyon, S. J., Fernandez-Castro, T., & Stencel, R.E., 1988, *AJ*, 95, 1817
- Lamers, H. J. G. L. M., & Cassinelli, J. P., 1999, *Introduction to Stellar Winds*. (Cambridge: Cambridge Univ. Press)
- Lee, H-W., 2000, *ApJL*, 541, L25
- Lee, H-W., 2009, *MNRAS*, 400, 2153
- Lee, H-W., 2012, *ApJ*, 750, 127
- Lee, H-W., Jung, Y-Ch., Song, I-O., & Ahn, S-H., 2006, *ApJ*, 636, 1045
- Lee, H-W., & Kang, S., 2007, *ApJ*, 669, 1156
- Lee, H-W., Kang, Y. W., & Byun, Y-I., 2001, *ApJL*, 551, L121
- Lee, H-W., & Lee, K-W., 1997, *MNRAS*, 287, 211
- Lee, H-W., Sohn, Y-J., Kang, Y. W., & Kim, H-I., 2003, *ApJ*, 598, 553
- McCuskey, S., 1965, *IAUC*, No. 1916
- Mürset, U., & Nussbaumer, H., 1994, *A&A*, 282, 586
- Nussbaumer, & H., Schild, H., 1981, *A&A*, 101, 118
- Nussbaumer, H., Schmid, H. M., & Vogel, M., 1989, *A&A*, 211, L27
- Nussbaumer, H., & Vogel, M., 1987, *A&A*, 182, 51
- Parimucha, Š., & Vaňko, M., 2005, *CoSka*, 35, 35
- Parimucha, Š., Chochol, D., Pribulla, T., Buson, L. M., & Vittone, A. A., 2002, *A&A*, 391, 999
- Pequignot, D., Baluteau, J. M., Morisset, C., & Boisson, C., 1997, *A&A*, 323, 217
- Puls, J., Vink, J. S., & Najarro, F., 2008, *A&ARv*, 16, 209
- Schild, H., 1989, *MNRAS*, 240, 63
- Schmid, H. M., 1989, *A&A*, 211, L31
- Schmid, H. M., 1997, in *Physical Processes in Symbiotic Binaries and Related Systems*, ed. J. Mikolajewska (Warsaw: Copernicus Foundation for Polish Astronomy), 21
- Schmid, H. M., & Schild, H., 1990, *MNRAS*, 246, 84
- Schmid, H. M., Krautter, J., Appenzeller, I., et al., 1999, *A&A*, 348, 950
- Schröder, K. P., 1985, *A&A*, 147, 103
- Seaquist, E. R., Krogulec, M., & Taylor, A. R., 1993, *ApJ*, 410, 260
- Seaquist, E. R., Taylor, A. R., & Button, S., 1984, *ApJ*, 284, 202 (STB)
- Sekeráš, M., & Skopal, A., 2012, *MNRAS*, 427, 979
- Skopal, A., 2006, *A&A*, 457, 1003
- Skopal, A., 2007, *New Astronomy*, 12, 597
- Storey, P. J., & Zeippen, C. J., 2000, *MNRAS*, 312, 813
- Vassiliadis, E., & Wood, P. R., 1993, *ApJ*, 413, 641
- Webster, B. L., & Allen, D. A., 1975, *MNRAS*, 171, 171
- Whitelock, P., Menzies, J., Feast, M. W., et al., 2009, *MNRAS*, 394, 795
- Whitelock, P., Menzies, J., Feast, M. W., Nsengiyumva, F., & Matsunaga, N., 2013, *MNRAS*, 428, 2216